Article:
Xu, Caiqi, Ma, Chao, Souri, Mohammad et al. (2024) Numerical Investigation of Thermal Management of a Large Format Pouch Battery Using Combination of CPCM and Liquid Cooling. Batteries. 113. ISSN: 2313-0105

https://doi.org/10.3390/batteries10040113

batteries

MDPI

Article

Numerical Investigation of Thermal Management of a Large Format Pouch Battery Using Combination of CPCM and Liquid Cooling

Caiqi Xu [1], Chao Ma [1], Mohammad Souri [2], Hadi Moztarzadeh [3], Mohammad Nasr Esfahani [4], Masoud Jabbari [1] and Elham Hosseinzadeh [4,*]

[1] School of Mechanical Engineering, University of Leeds, Leeds LS2 9JT, UK; m.jabbari@leeds.ac.uk (M.J.)
[2] Harvard John A. Paulson School of Engineering and Applied Sciences, Harvard University, Allston, MA 02134, USA
[3] Advanced Propulsion Centre, Coventry CV4 7AL, UK
[4] School of Physics, Engineering and Technology, University of York, York YO10 5DD, UK
* Correspondence: eli.hosseinzadeh@york.ac.uk

Abstract: As electric vehicles (EVs) gain market dominance, ensuring safety during the battery usage is crucial. This paper presents a new thermal management approach to address the battery heat accumulation challenge through a novel combination of composite phase change material (CPCM) with liquid cooling systems. An optimised hybrid cooling model is developed to evaluate the proposed battery thermal management system (BTMS) under high-temperature and high-power conditions. Benchmark studies are conducted to assess the impact of inlet position, inlet flow rate, and flow channel distribution on the cooling performance to achieve a uniform temperature distribution within the battery. The optimised BTMS, consisting of a five-cell battery pack, demonstrates a maximum temperature of 41.15 °C and a temperature difference of 4.89 °C in a operating condition at 36 °C with a discharge rate of 3 C. The BTMS outperforms the initial model, reducing the maximum temperature by 1.5%, temperature difference by 5%, and liquid fraction by 13%, with a slight (1.3%) increase in weight. The cooling performance is most efficient at a liquid flow rate of 0.1 m/s, minimising energy consumption. The proposed BTMS with CPCM-3 is also sufficient enough to keep the battery pack under a thermal runaway event. Overall, the theoretical simulation highlights the BTMS's ability to effectively control battery temperatures and temperature differences, ensuring safe operation during high-temperature and high-power conditions in practical EV usage.

Keywords: lithium-ion battery; battery thermal management system; composite phase change material; liquid cooling

Citation: Xu, C.; Ma, C.; Souri, M.; Moztarzadeh, H.; Nasr Esfahani, M.; Jabbari, M.; Hosseinzadeh, E. Numerical Investigation of Thermal Management of a Large Format Pouch Battery Using Combination of CPCM and Liquid Cooling. *Batteries* **2024**, *10*, 113. https://doi.org/10.3390/batteries10040113

Academic Editor: Thomas Wetzel

Received: 11 December 2023
Revised: 19 March 2024
Accepted: 20 March 2024
Published: 22 March 2024

1. Introduction

Due to the significant impact of carbon emissions on the environment [1], in order to reduce carbon emissions, the use of electric vehicles will be more prevalent compared to traditional combustion ones in future. This is because electric vehicles use batteries as a power source, which can reduce the use of fossil fuels, achieve sustainable development, and reduce environmental pollution [2]. Using lithium-ion batteries (LIBs) as an energy storage system for electric vehicles is highly suitable, offering a high energy density and enabling electric vehicles to have a more extended driving range. They can maintain a high level of performance even after multiple charge–discharge cycles, thus having a longer lifespan. Compared to other types of batteries such as traditional lead-acid batteries, LIBs have a lighter weight [3,4]. However, operating at high temperatures can have adverse effects on LIBs. High temperatures accelerate the aging process of the batteries and shortening their lifespan. Additionally, prolonged operation at high temperatures can lead to corrosion and damage to the internal materials of the batteries and even pose

thermal runaway and safety hazards. Therefore, the optimal operating temperature for LIBs is between 20–40 °C [5,6]. In electric vehicles, multiple battery cells are usually combined to form a battery pack to provide sufficient electrical energy. Suppose there is a significant temperature difference between these battery cells. In that case, it may lead to thermal runaway in some cells, particularly under high-temperature conditions, thus causing severe safety issues. However, controlling the temperature variation across the batteries within 5 °C helps maintain thermal balance within the battery pack and reduces the risk of thermal runaway [7]. Charging and discharging cycles LIBs generate a significant amount of heat, and techniques to dissipate the generated heat is a critical issue [8]. If this heat is not promptly released during the aforementioned process, heat accumulation can occur, leading to overheating of the battery pack and causing the adverse effects mentioned above [9].

In the era of the increasing popularity of electric vehicles, designing a battery thermal management system (BTMS) that has a good performance, minimises energy losses, and ensures safety has become increasingly crucial for the safety and reliability of electric vehicles. BTMS can be divided into two main categories of cooling methods: internal material modifications and external environment modifications [10]. In terms of internal material modifications, the thickness and materials of the electrodes can be changed to reduce the heat generation of the battery [11–13]. In terms of internal material modifications, the thickness and materials of the electrodes can be changed to reduce the heat generation of the battery [10].

For battery packs operating under high temperature and high power conditions, relying solely on active cooling would require the active cooling method to constantly work and dissipate heat to ensure safety, resulting in a certain amount of energy loss [7,14,15]. On the other hand, using passive cooling alone is insufficient for effectively and rapidly removing heat from the battery pack at high-temperature and high-current environments [16–19].

Over recent years, focus switched on the use of phase change material (PCM) cooling. It is found that PCM significantly improves the temperature's uniform distribution in a battery pack [20]. Most of the literature has focused on organic paraffin due to its properties such as safety, reliability, and low cost. These PCMs, however, are characterised by low thermal conductivity. Therefore, the heat transfer process will be slower than needed and heat will accumulate inside the batteries. An effective approach found is the use of paraffin based composite PCMs (CPCM) modified with metal and carbon-based materials [21]. Paraffin has a wide variety of advantages such as low cost, chemical stability, and small volume change during melting. The added carbon and metal-based materials will increase the thermal conductivity in addition to other properties [22]. Using PCMs/CPCMs only, however, is not sufficient for cooling of large format batteries with a high discharge rate, and hence, hybrid approaches (using liquid cooling/cold plate) are proposed to be a better alternatives [23].

Zhao et al. [24] developed a BTMS for cylindrical LIB packs. They used a combination of copper foam/paraffin composite phase change material (CPCM) and liquid for hybrid cooling. Their study indicated that using CPCM resulted in better cooling performance than using pure phase change materials (PCM). Furthermore, liquid cooling effectively preheated the battery and cooled it in high-temperature environments.

Zhang et al. [25] implemented a BTMS using PCM and liquid cooling and simulated the conditions under which this BTMS could maintain the battery's operating temperature through the latent heat of PCM while the liquid cooling removed heat, thereby avoiding thermal runaway. The study also discussed the possibility of reducing the occurrence of thermal runaway by optimising the thermal conductivity of PCM and the flow rate of the liquid. However, the article did not consider the potential energy loss that may arise from increased liquid flow rates.

Fan et al. [26] proposed a BTMS that utilises phase change materials and liquid cooling with a multi-stage Tesla valve using liquid pipelines. By modifying the flow channel shape, they achieved a 79.9% reduction in pump energy consumption while achieving good cooling performance and lower temperature differentials. Additionally, it was found that this system could prolong the battery's warmth-holding time in low-temperature environments. However, the study overlooks the potential manufacturing cost and material issues associated with the complexity of the flow channel structure.

Kong et al. [27] introduced a BTMS that utilises hybrid cooling, combining CPCM and liquid cooling. They proposed a liquid cooling control strategy that controls the velocity and temperature of the liquid through CPCM and ambient temperature, thereby improving the energy utilisation efficiency of the system and avoiding energy loss. However, the study did not consider the safety issues that may arise from temperature variations in the battery pack when the control strategy fails.

Most of the research studies on BTMS utilising PCMs/CPCMs and liquid cooling methods have focused on understanding the cooling performance of the system during the charging/discharging process of LIBs. However, there is a lack of comparative sturdy on different CPCMs and their performance with different cooling configuration, and their behaviour under harsh cases like thermal runaway events.This paper initially presents a comparative analysis to select suitable CPCM materials for passive cooling. Subsequently, a hybrid cooling model is developed, and the inlet positions and and shape of flow channels are optimised with investigating four different configurations. Numerical simulations, furthermore, are conducted to evaluate the cooling performance of the BTMS, analysing the influence of liquid flow rate on cooling performance, and determine the optimal flow rate to ensure efficient cooling without unnecessary energy loss. The cooling performance of the system is also simulated when the active cooling method fails. The optimised model and configuration is further developed to study the LIB pack performance under WLTP drive cycle and a thermal runaway case study.

2. LIB Cell Specification

The commercial 53 Ah large format pouch cells with dimension of $x \times y \times z = 0.225\ \text{m} \times 0.225\ \text{m} \times 0.0118\ \text{m}$ manufactured by XALT ENERGY (Midland, MI, USA) is used in this study for investigating the proposed hybrid BTMS. The chemistry of cathode is $LiNi_xMnyCo_{1-x-y}O_2$ (NMC) and the anode is made of graphite (LiC_6). For this LIB cell, the operating temperature range is considered in a range of $-20\ ^\circ\text{C}$ to $60\ ^\circ\text{C}$ for discharge, with a lower and upper limit voltage of 2.7 V during the discharge process. From the cells' potential measurements, the open circuit voltage (OCV) was collected at 1 C discharge from 100% to 0% state of the charge (SOC), where 0% SOC corresponds to reaching the cut-off voltage of 2.7 V. The terminal voltage of the cells was assessed at the end of the rest period. During the OCV measurement, the cell was discharged at 1 C with a 4% SOC increment until it hit the cut-off voltage of 2.7 V. Each step was followed by a period of 4 h rest to let the voltage stabilise. The cell terminal voltage was measured at the end of each step. To initiate the cell testing, the cells underwent a preconditioning process. This involved discharging the cells at a rate of 1 C until the cells reached a limit of 2.7 V. Following this, the cells rested for a duration of 4 h to achieve equilibrium. Subsequently, the cells were subjected to charging under a condition of constant current-constant voltage (CC-CV). In the constant current (CC) section, the cells were charged at a rate of 1 C until reaching a voltage of 3.6 V. The voltage was then maintained at 3.6 V until the current decreased to C/20. This was followed by a 4 h period of rest. Following the preconditioning of the cells, they were discharged at constant C-rates until a voltage limit of 2.7 V was reached. The measured OCV and the terminal voltage at 3 C are shown in Figure 1 [28].

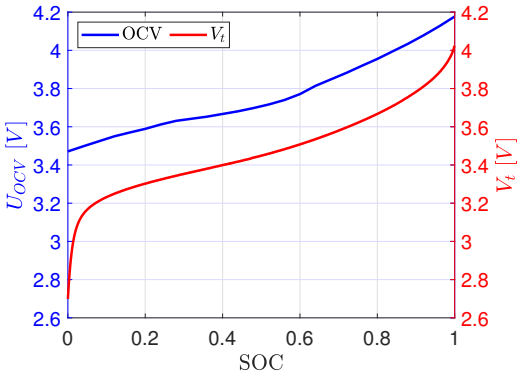

Figure 1. Experimental measurements of OCV, and the terminal voltage as a function of SOC at the end of 3 C discharge (at 25 °C)—adapted with permission from [28].

3. Numerical Model

3.1. LIB Cells

The effectiveness of the energy equation for predicting the thermal behaviour of battery cells has been validated and confirmed by many studies in open literature [29]. Hence, energy equations that only involve heat conduction are adapted for the 3-D thermal simulation of the cell. In this regard, the energy equations for a LIB cell can be expressed

$$\rho c_P \frac{\partial T}{\partial t} = \frac{\partial}{\partial x}\left(k_x \frac{\partial T}{\partial x}\right) + \frac{\partial}{\partial y}\left(k_y \frac{\partial T}{\partial y}\right) + \frac{\partial}{\partial z}\left(k_z \frac{\partial T}{\partial z}\right) + \dot{q}''', \tag{1}$$

where ρ is the density, c_P is the specific heat capacity, k is the thermal conductivity (subscripted by different directions), and $\dot{q}'''$ is the overall heat generation of the LIB. For a LIB cell, the overall heat generation term consists of the cell heat generation, $\dot{q}'''_{\text{cell}}$, and the heat generation due to tabs (positive and negative), $\dot{q}'''_{\text{tabs}}$, and thus $\dot{q}''' = \dot{q}'''_{\text{cell}} + \dot{q}'''_{\text{tabs}}$. The heat generation in the LIB cell with irreversible and reversible heat is as follows

$$\dot{q}'''_{\text{cell}} = \left[I(OCV - V_t) - I\left(T\frac{d(OCV)}{dT}\right)\right] \times \frac{1}{V_{\text{cell}}}, \tag{2}$$

in which the irreversible heat generation—first term—is due to Joule heating, the reversible heat—second term—is due to entropy change, and V_{cell} is LIB cell volume. In this study, we only consider the dominant Joule heating, where the experimental data at 3C is inputted—the fitted function is illustrated in Figure 2.

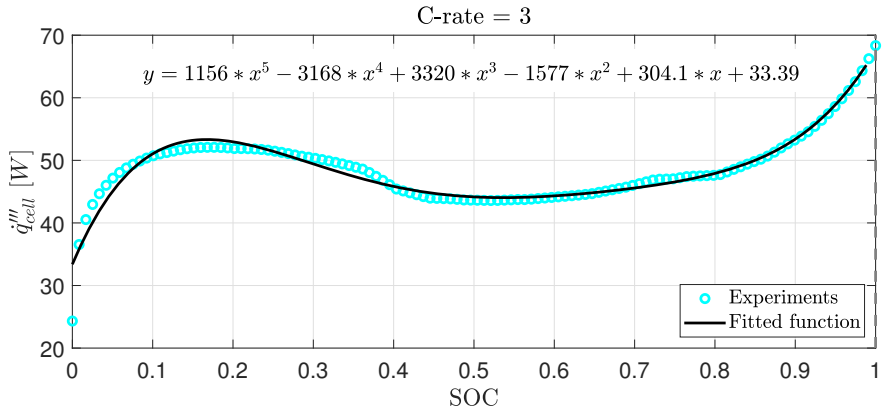

Figure 2. Heat generation curve inside a 53 Ah LIB cell (with a natural convection state, h_∞ = 6 W/m^2·K) and the corresponding fitted functions at discharge rate of 3C — adapted with permission from [30].

The heat generation of tabs is mainly due to the inherent electrical resistance, R_{tab}, and the contact resistance, R_c, as

$$\dot{q}'''_{\text{tab}} = \left[I^2(R_{\text{tab}} + R_c)\right] \times \frac{1}{V_{\text{tab}}}, \tag{3}$$

which is applied for both positive and negative tabs, and V_{tab} is the volume of tabs. The thermo-electrical properties of the LIB cell and the tabs are summarised in Table 1.

Table 1. Thermal and electrical properties of the LIB cell and the tabs—adapted with permission from [28].

Domain	ρ [kg/m^3]	c_P [J/kg·K]	k [W/m·K]	R_c [Ω]
Cell	2551.7	1100	$k_x = k_y = 28$, $k_z = 0.28$	–
Tab(+)	7987	381	387.6	6.37×10^{-5}
Tab(−)	7987	381	387.6	3.40×10^{-5}

3.2. CPCM

Modelling of CPCMs is similar to PCMs with two main approaches the enthalpy method and the temperature method [31]. In this study, we adapted the enthalpy method, where the energy equation of solid and liquid phases are solved in one expression [32]. The thermophysical properties of CPCM, like density and specific heat, are assumed constant, and the viscosity of CPCM is infinite—ignoring liquid phase flow. The energy equations of the CPCMs domain are then

$$\rho_{\text{CPCM}} \frac{\partial H}{\partial t} = k_{\text{CPCM}} \left(\frac{\partial^2 T}{\partial x^2} + \frac{\partial^2 T}{\partial y^2} + \frac{\partial^2 T}{\partial z^2} \right), \tag{4}$$

where the total enthalpy, H, is

$$H = h + \Delta H, \tag{5}$$

which combines the sum of sensible heat, h,

$$h = \int_{T_0}^{T} c_{\text{CPCM}} dT, \tag{6}$$

and the phase change enthalpy is $\Delta H = f\gamma$, where γ is the latent heat of fusion, and the liquid fraction f between the solidus (T_s) and liquidus (T_l) temperature of the CPCM is calculated by [33]

$$f = \begin{cases} 0 & T < T_s \\ 1 & T > T_l \\ \frac{T - T_s}{T_l - T_s} & T_s < T < T_l \end{cases} \tag{7}$$

Three different CPCM materials [34–36] were selected as a comparison through numerical simulations—summarised in Table 2.

Table 2. Material characteristics of the three different CPCMs—adapted with permission from [34–36].

Materials	ρ [kg/m^3]	c_P [J/kg·K]	k [W/m·K]	H [J/kg]	T_s [°C]	T_l [°C]
CPCM-1	895	1910	12	160,000	32	38
CPCM-2	1130	1600	4.27	127,000	33.9	47.6
CPCM-3	880	2100	7.62	210,000	36	40

3.3. Liquid Cooling

This article uses cooling channels and a 50% water-ethylene glycol mixture as the active cooling structure and coolant. This mixture is used because it has a freezing point of −37.9 °C, which is lower than water's, meeting the requirements for use under extremely low temperatures in winter [37]. The maximum velocity of water flow is 0.14 m/s, which results in Reynolds number less than 2300 based on

$$Re = \frac{\rho_c v_c d_c}{\mu_c}, \tag{8}$$

where ρ_c represents the density of the coolant, v_c is the flow velocity of the coolant, μ_c is the coolant viscosity, and d_c is the hydraulic diameter of the channel. The energy equation for the aluminum cooling plate (where channels are going through) with constant thermal conductivity is

$$\rho_{al} c_{al} \frac{\partial T_{al}}{\partial t} = k_{al} \left(\frac{\partial^2 T}{\partial x^2} + \frac{\partial^2 T}{\partial y^2} + \frac{\partial^2 T}{\partial z^2} \right), \tag{9}$$

where ρ_{al}, c_{al}, and k_{al} are the density, specific heat capacity, and thermal conductivity of the aluminum cold plate, respectively. The governing equations related to liquid coolant, including mass conservation, momentum conservation, and energy conservation laws, are shown below [38].

$$\nabla \cdot \mathbf{u} = 0, \tag{10}$$

$$\rho_c \frac{d\mathbf{u}}{dt} = -\nabla p + \mu_c \nabla^2 \mathbf{u}, \tag{11}$$

$$\rho_c c_c \left[\frac{\partial T_c}{\partial t} + \nabla \cdot (\mathbf{u} T_c) \right] = k_c \nabla^2 T_c, \tag{12}$$

in which $\mathbf{u}$ is the velocity vector, p is pressure, k_c is the thermal conductivity of the coolant, and c_c is the specific heat capacity of the coolant. The thermo-physical properties of different materials used in this paper are listed in Table 3.

Table 3. Properties of materials used in this study—adapted with permission from [37,39].

Materials	ρ [kg/m^3]	c_P [J/kg·K]	k [W/m·K]	μ [Pa·s]
Air	1.225	1006	0.0242	1.79×10^{-5}
Coolant	1063.66	3358	0.394	3.78×10^{-3}
Aluminium	2719	871	202.4	-

3.4. Simulation Domain

In this study, a 5-cell LIB model with positive (P) and negative (N) tabs—Figure 3—was first established, with a thickness of 5 mm for the CPCM. This model is used to run a comparative analysis between the three CPCM materials—summarised in Table 2—in terms of their cooling performance.

After selecting the best CPCM material, the thermal performance of the combination of CPCM and liquid cooling was optimised, and the performance of BTMS was simulated when active cooling failed. Four BTMS configurations were proposed and analysed in this study: (1) CPCM and liquid cooling with S-shaped distributed liquid channels; (2) changed the positions of liquid inlet and outlet for configuration (1); (3) added layering to the flow channels of configuration (2); (4) added liquid and CPCM for cooling at the top and bottom of configuration (3) and curved the channel corners—shown in Figure 4a–d, respectively.

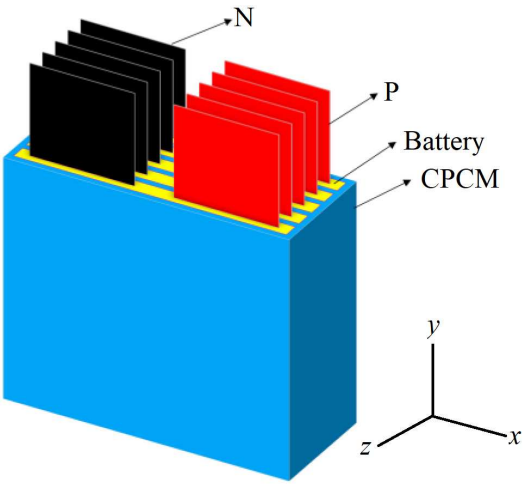

Figure 3. The simulation domain for the passive cooling model of the CPCM and the LIB cells.

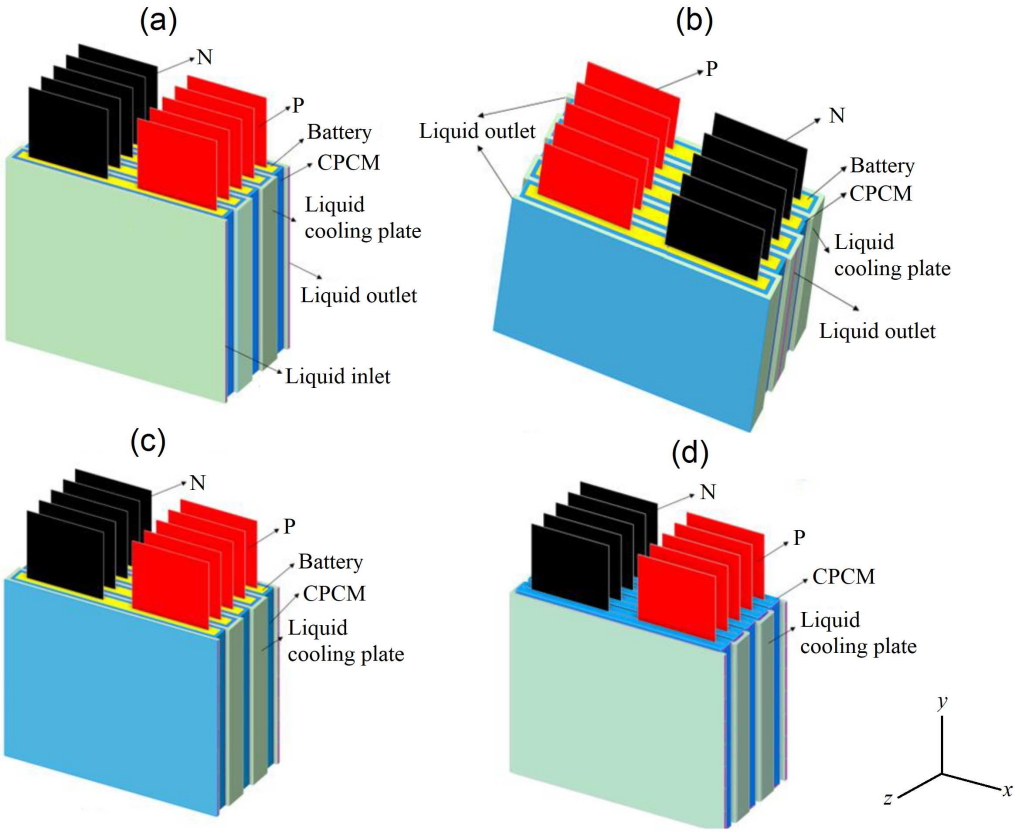

Figure 4. Four different BTMS configurations analysed in this study, (**a**) configuration (1), (**b**) configuration (2), (**c**) configuration (3), and (**d**) configuration (4).

The CPCM thicknesses in configurations (1)–(4) are 3 mm. The thickness of the liquid cooling plate is 1 mm, and the width of the flow channel is 2 mm. In configuration (3), the flow channel is divided into 8 layers, each with a height of 25 mm. The cooling plate thickness between the layers is consistent 3 mm, while the cooling plate in the center has a thickness of 4 mm. In configuration (4), CPCM and liquid cooling are added at the top and bottom. The opening thickness at the top, used for tab placement, is 1.8 mm. There are two liquid flow channels at the top, spaced 1 mm apart, with dimensions of $x \times y \times z$ = 231 mm × 1 mm × 6 mm; the bottom has one liquid flow channel with dimensions of $x \times y \times z$ = 231 mm × 1 mm × 8 mm.

3.5. Boundary Conditions

For the tabs and surfaces exposed to the ambient air, the convective boundary condition is assumed. Contact resistance between CPCM and LIB or cooling plate is neglected [31], and radiation heat transfer is disregarded [32]. The ambient temperature, the initial temperature of the LIB, CPCM, and the cooling plate are all set to 26.85 °C. For any two media (Θ), with contact surface(s), conservation of energy is assumed as

$$-k_{\Theta_i}\frac{\partial T}{\partial \mathbf{n}} = k_{\Theta_{i+1}}\frac{\partial T}{\partial \mathbf{n}}, \qquad \Theta_{i=1:5} \in \{\text{LIB, Tabs, CPCM, Aluminium, Coolant}\} \tag{13}$$

where **n** is the normal vector. Here, the convective boundary condition for any medium with the surface(s) in contact with air of temperature T_0 is

$$-k_{\Theta_i}\frac{\partial T}{\partial \mathbf{n}} = h(T - T_0), \qquad \Theta_{i=1:4} \in \{\text{LIB, Tabs, CPCM, Aluminium}\}, \tag{14}$$

and h is the heat transfer coefficient, with a value of 6 W/m^2·K in this study.

3.6. Mesh Sensitivity Analysis and Validation

Geometrical design, meshing, and solving the governing equations have been implemented in the commercial software Ansys Fluent 2023 R1. The BTMS designed in this study includes complex structures and physics involving solid-fluid heat transfer, laminar flow, and phase change, which require more attention on meshing. Especially in areas where two (or more) media are coupled, a finer mesh is necessary. Through the grid independence evaluation with a flow speed of 0.1 m/s, the results demonstrate that the simulation is stable and independent of the mesh with 1,290,307 control volumes—c.f. Figure 5. A grid refinement is used in CPCM medium and corresponding contact surfaces, where the surface mesh size is set in the range of 1–3 mm, with 2 cells per gap. The maximum length of the body mesh is 3 mm.

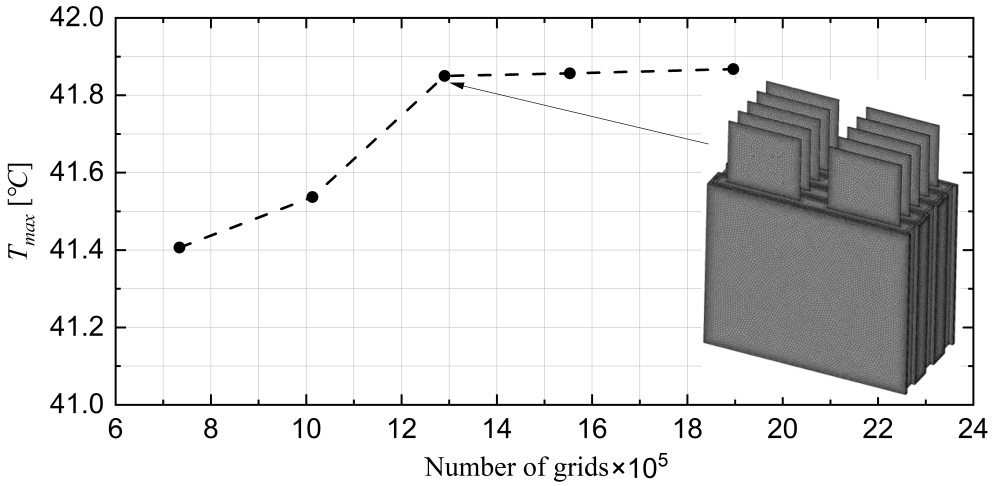

Figure 5. Mesh independence of the 3-D model with respect to the number of grids, and an example of mesh topology.

To further validate the modelling tool used in this paper, the maximum temperature of the single-cell LIB during 3 C discharge was compared with the experimental data from Hosseinzadeh et al. [28]. The results of comparison—shown in Table 4—confirms that the modelling tool used in the manuscript is capable of predicting temperature changes within LIBs relatively good.

Table 4. Comparison of maximum temperature for a single-cell LIB under 3 C discharge rate against experimental data (adapted with permission) from [28].

t [s]	$T_{max}^{exp.}$ [°C]	$T_{max}^{num.}$ [°C]	Error [%]
30	26.9	25.94	3.56
400	36.1	33.13	8.22
800	42.6	42.18	0.98
1100	49.1	51	−3.87

4. Results and Discussion

4.1. Comparative Selection of CPCMs

From the results shown in Figure 6a, it can be observed that the minimum temperature of the battery pack is achieved when cooling is performed using CPCM-1 material. The minimum temperature difference and liquid fraction are obtained when cooling is performed using CPCM-3—see Figure 6b. In case of using CPCM-1 material, the temperature difference of the battery pack is more than 5 °C and the liquid fraction is maximum. However, the maximum temperature of the battery pack is only 2 °C lower when CPCM-3 material is used. It is worth noting that when CPCM-3 material is used, the temperature difference of the battery pack is less than 5 °C and the degree of liquefaction of CPCM is minimum. The maximum temperature of the battery pack does not exceed 42 °C. Based on the above comparison, it can be concluded that the cooling performance is better by using CPCM-3 material. Therefore, CPCM-3 material is selected as the passive cooling system for the BTMS for the rest of the investigations in this work (unless mentioned otherwise).

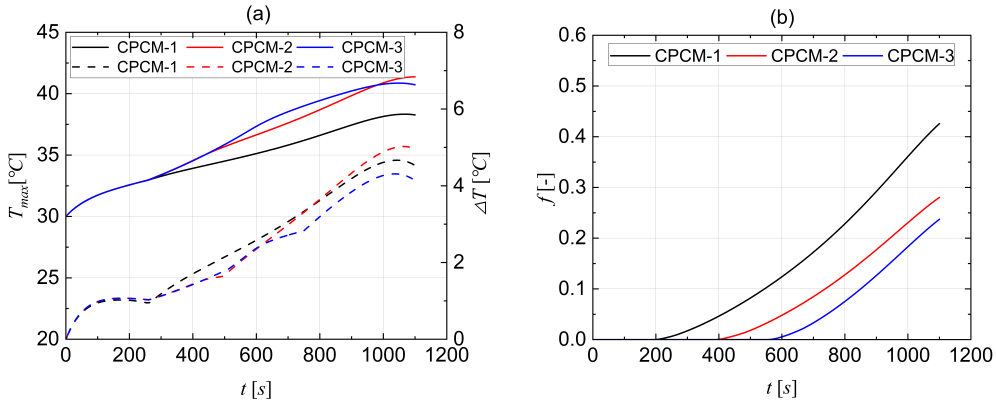

Figure 6. Results at a temperature of 26.85 °C and the 3 C rate of the cell showing (**a**) maximum temperature (solid lines) and temperature difference (dashed lines), and (**b**) liquid fraction, over time.

4.2. Performance of the Hybrid Cooling Model

Results of the configuration (1) BTMS simulation are presented in Figure 7. It can be seen that with the use of configuration (1) for BTMS when the time reaches 980 s, the temperature difference of the battery pack exceeds 5 °C, which may lead to thermal runaway and safety issues [7]. Therefore, it is necessary to optimise this configuration. When the time reaches 1050 s, there is a reduction in the maximum temperature as well as the temperature variation. This is attributed to a reduction in the heat generation rate, which falls below the cooling rate [39]. Additionally, an examination of the battery's heat generation reveals that when the SOC is below 0.1, the heat generation rate drops rapidly, which could have contributed to the reduction of the temperature difference and maximum temperature.

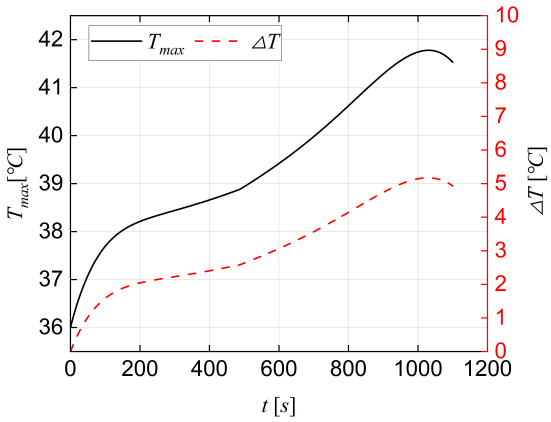

Figure 7. The maximum temperature (solid lines) and temperature difference (dashed lines) for configuration (1) at 3 C discharge rate and using CPCM-3.

From the top view of the LIB pack for configuration (1)—shown in Figure 8a—it can be seen that the temperature is lower for the LIB pack closer to the inlet of the coolant on the left side, and higher when the battery pack is closer to the outlet of the coolant. This is due to the fact that the coolant takes away heat from the LIBs while travelling through the channels, resulting in a temperature rise of its own, and reducing the cooling capacity for the LIBs.

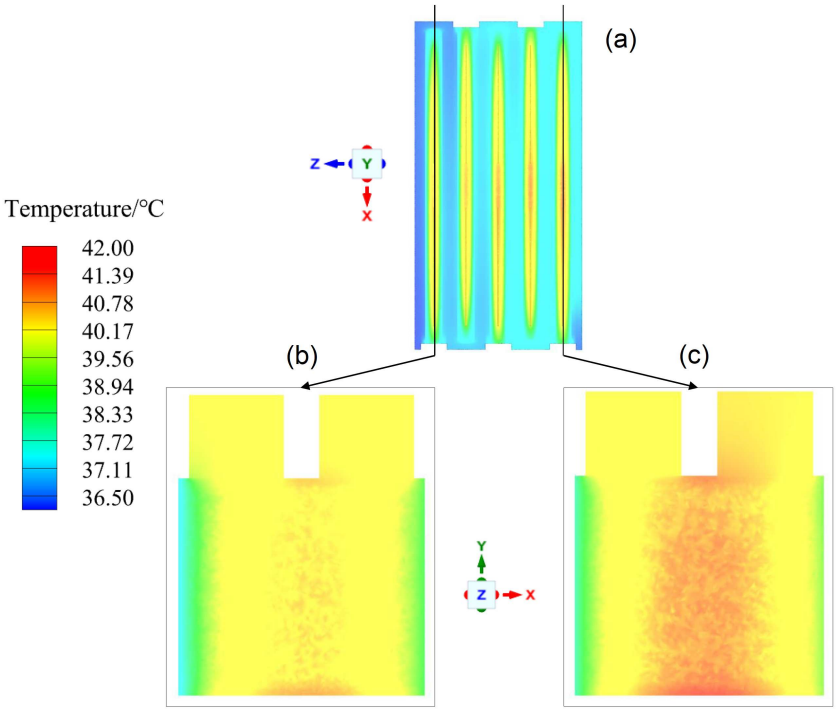

Figure 8. Temperature distribution of configuration (1) at 3 C discharge rate and using CPCM-3 (**a**) from the top view of the LIB pack, (**b**) of the LIB near the coolant inlet, and (**c**) of the LIB near the coolant outlet.

By examining the cross-sections of the two LIBs near the inlet and outlet, as shown in Figure 8b,c, it can be seen that the battery near the outlet has a higher temperature, and the temperature at the top and bottom is higher than in the middle. This is because the top and bottom are in contact with air and cannot dissipate heat quickly, resulting in excessive temperature differences. The temperature at the top is higher because the lower

temperature coolant, due to the gravitational force, reaches the bottom first, causing the temperature below to be higher than the temperature above.

To improve the uneven temperature distribution of the batteries near the inlet and outlet, configuration (2) is proposed, which involves changing the positions of the coolant inlet and outlet. The inlet is placed in the middle of the LIB pack to maximise the average temperature between the cells. In order to reduce the influence of gravity on the coolant flow direction, configuration (3) was suggested by layering the flow channels to allow for a more uniform distribution of coolant within the BTMS, thus achieving better cooling performance. Finally, to address the issue of the highest temperatures being unable to dissipate quickly at the top and bottom in configuration (1), configuration (4) was proposed by using CPCM in conjunction with the coolant with curved cooling channels.

The comparison of the cooling performance of different configurations is depicted in Figure 9. It is seen that using configuration (4) leads to the lowest maximum temperature and temperature difference in LIBs, and the lowest liquid fraction in CPCM. Therefore, configuration (4) exhibits the best cooling performance as the BTMS. In this case, the maximum temperature of the LIB pack is 41.40 °C, and the maximum temperature difference is 5.13 °C, which is close to 5 °C (the ideal temperature difference).

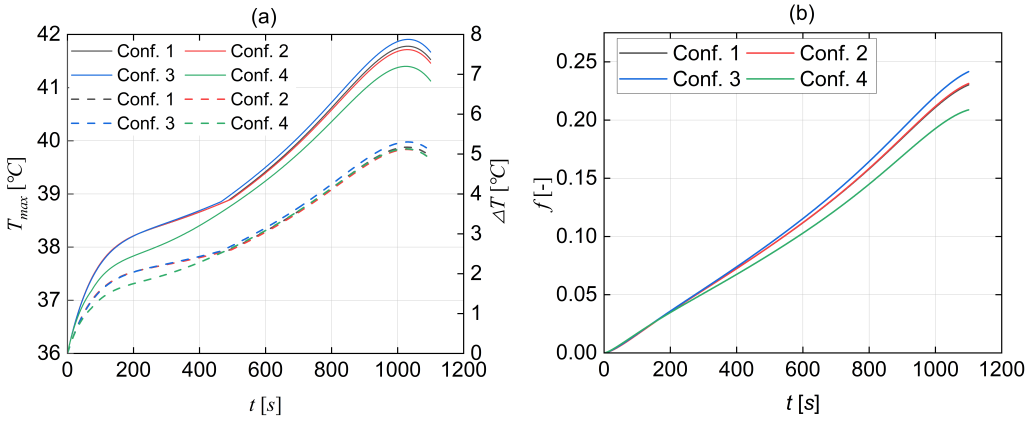

Figure 9. Results of four different configurations (Conf.#) at a temperature of 36 °C and the 3 C rate of the cell using CPCM-3 showing (**a**) maximum temperature (solid lines) and temperature difference (dashed lines), and (**b**) liquid fraction, over time.

From the top view of the LIB pack shown in Figure 10, it can be observed that the temperature distribution among the batteries is significantly improved after iterative design optimisation. Figure 10b represents the temperature distribution of configuration (4), where it can clearly be seen that the temperature distribution of the batteries near the inlet and outlet is greatly improved, resulting in a more uniform temperature distribution among the LIB cells. It is worth mentioning that the curved channels in configuration (4) reduce the occurrence of liquid backflow and enhance the efficiency of liquid flow, thereby reducing energy (power) consumption.

The temperature distribution of the cross-section of the LIB Pack closest to the coolant outlet for different configurations is illustrated in Figure 11. The comparison of Figure 11a–c demonstrate that the arrangement of the flow channels contributes to a more consistent longitudinal temperature distribution within the LIB pack. Through the comparison of Figure 11a–d, it is evident that the addition of CPCM and coolant at the upper and lower sections successfully facilitates heat dissipation from the LIB pack, resulting in a decreased temperature disparity among the cells. Consequently, the highest temperature within the battery pack is registered near the centre of the cells.

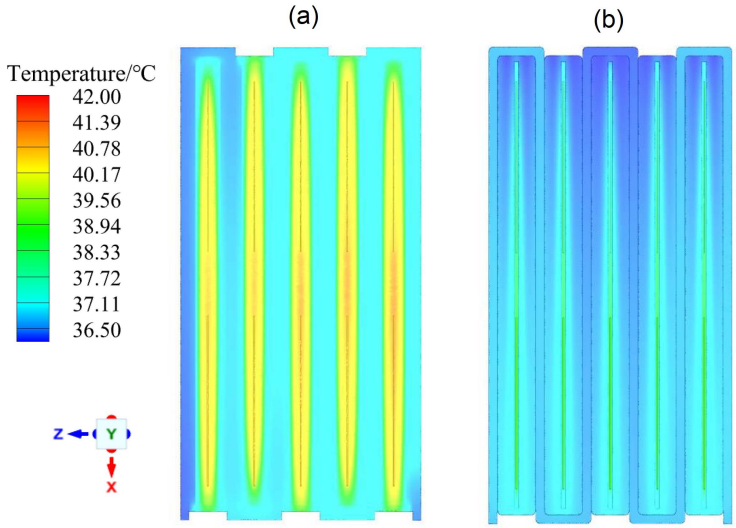

Figure 10. Temperature distribution of the LIB pack at 3 C discharge rate and using CPCM-3 for (**a**) configuration (1), and (**b**) configuration (4).

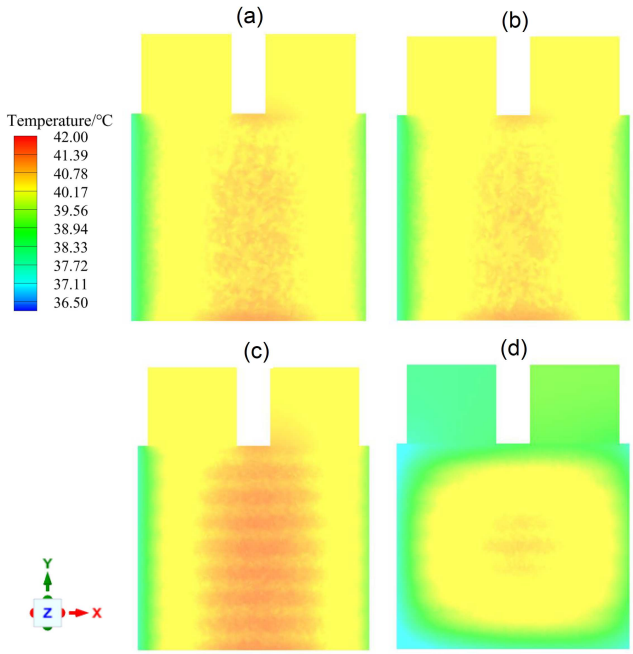

Figure 11. Temperature distribution along the longitudinal interface of the LIB pack closet to the coolant outlet at 3 C discharge rate and using CPCM-3 for (**a**) configuration (1), (**b**) configuration (2), (**c**) configuration (3), and (**d**) configuration (4).

From Figure 11, it is evident that the temperature in Configuration (3) is higher than Configurations (1) and (2). This is due to the use of layered aluminum (3–4 mm thick) in the flow channel, resulting in weakened longitudinal heat dissipation. As the electrode's heat dissipation primarily occurs through longitudinal cooling, this leads to a slightly higher internal heat within the battery. However, the advantage of this approach is the reduction in the overall weight of the battery pack, resulting in a more even temperature distribution. To mitigate heating at the top and bottom, configuration (4) demonstrates a decrease in the overall temperature and temperature difference of the battery pack after adding cooling materials to the top and bottom. The electrode temperature also decreases significantly, ensuring uniformity within the battery pack.

Based on the aforementioned results, it can be concluded that the optimised configuration (4) successfully satisfies the safety requirements of the LIB pack—during regular

BTMS operation—effectively preventing the risk of thermal runaway when exposed to a high-temperature environment of 36 °C and discharged at a rate of 3 C, this configuration exhibits a maximum battery pack temperature of 41.15 °C, maintaining a temperature difference within the acceptable limit of 5 °C. Compared to the initial design (configuration (1)), configuration (4) offers several improvements. It reduces the maximum temperature by 1.5%, decreases the maximum temperature difference by 2.5%, and reduces the liquid fraction by 15%. In addition, it only increases the weight by 1.2%. Overall, configuration (4) not only enhances the safety of the LIB pack but achieves better cooling performance with only a slight increase in weight.

4.3. Optimising BTMS Energy Consumption

To reduce the energy consumption of the BTMS while maintaining the LIB pack within normal operating temperatures and temperature differences, it is essential to explore the coolant flow rate that results in the lowest energy consumption. This study examined the cooling performance and energy consumption of the BTMS at various flow rates of 0.02 m/s, 0.04 m/s, 0.06 m/s, 0.08 m/s, 0.1 m/s, 0.12 m/s, and 0.14 m/s.

As depicted in Figure 12a, the results indicate that when the coolant flow rate is less than 0.06 m/s, the maximum temperature difference within the battery pack exceeds 5 °C, potentially leading to a state of thermal runaway and posing significant risks. Therefore, to ensure the safety of the battery pack, the coolant flow rate must be maintained above 0.06 m/s.

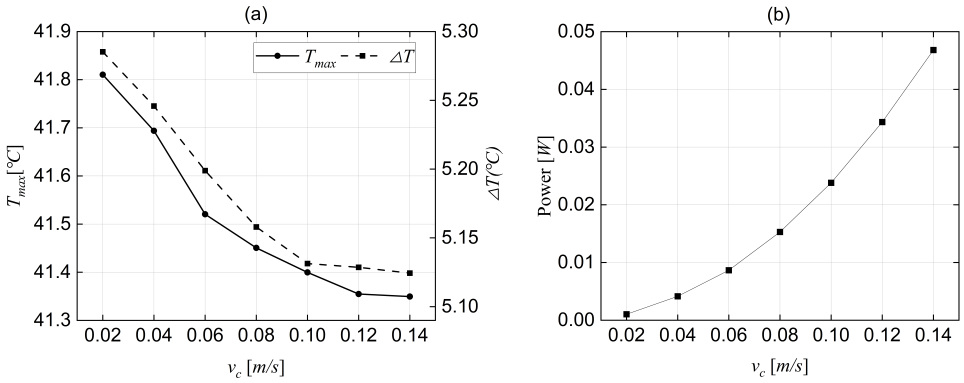

Figure 12. Cooling performance and energy consumption of BTMS at different coolant flow rates—at 3 C discharge rate and using CPCM-3—indicating (**a**) BTMS cooling performance (maximum temperature and maximum temperature difference), and (**b**) BTMS energy consumption.

Based on the combined analysis of Figure 12a,b, it is evident that when the coolant flow rate is set to 0.1 m/s, the LIB pack's maximum temperature and temperature difference are both at relatively low values. Additionally, at this flow rate, the energy consumption of the BTMS is only 0.024 W. However, as the coolant flow rate continues to increase, the energy consumption of the BTMS rises rapidly, while the improvement in the BTMS cooling performance becomes insignificant. Consequently, we can conclude that, for this BTMS setup, setting the coolant flow rate to 0.1 m/s can effectively reduce energy losses while ensuring that the LIB pack operates within a safe temperature range.

4.4. Safety of BTMS

To assess the safety of the BTMS under hybrid cooling conditions, simulations were conducted to model the scenario of active cooling failure. In this situation, the flow velocity of the coolant is reduced to 0 m/s while the coolant remains present within the flow channels. The results are shown in Figure 13. It can be seen that even when active cooling is off, utilising passive cooling alone is still capable of maintaining the temperature difference of the LIB pack at 5 °C or below. This ensures the normal and safe operation of the LIB pack under high-temperature conditions (36 °C) and a 3 C discharge rate. The

maximum temperature recorded was 41.7 °C, with the highest liquid fraction in the BTMS reaching 0.41.

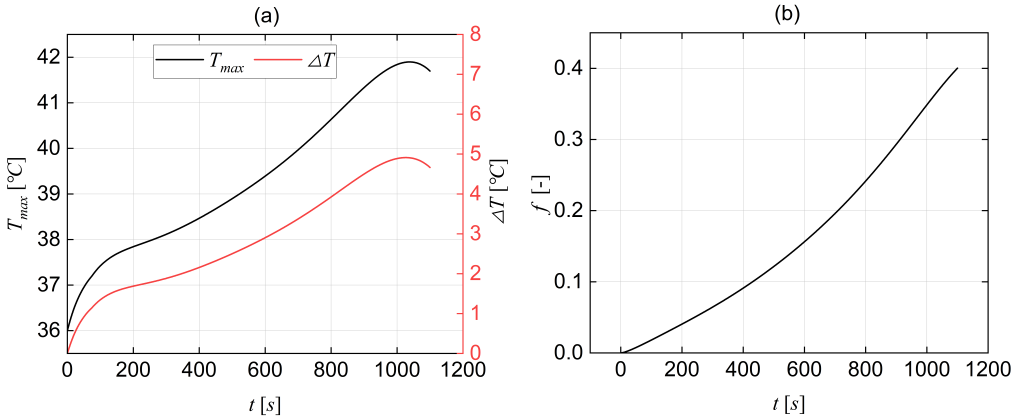

Figure 13. BTMS cooling performance in the event of active cooling failure at 3 C discharge rate and using CPCM-3 showing (**a**) BTMS cooling performance, and (**b**) BTMS liquid fraction.

4.5. Configuration (4) Performance under a Drive Cycle

As the best performing case, configuration (4) is used for further analysis of the LIB pack under the Worldwide Harmonised Light Vehicle Test Procedure (WLTP—class 3) drive cycle. The experimental data for heat generation of the LIB cells, negative and positive tabs—from [28]—are illustrated in Figure 14. A user-defined function (UDF) is used to hook the heat generation variations to Ansys to analyse the cooling performance of the configuration (4) BTMS when employing three different CPCMs (from Table 2).

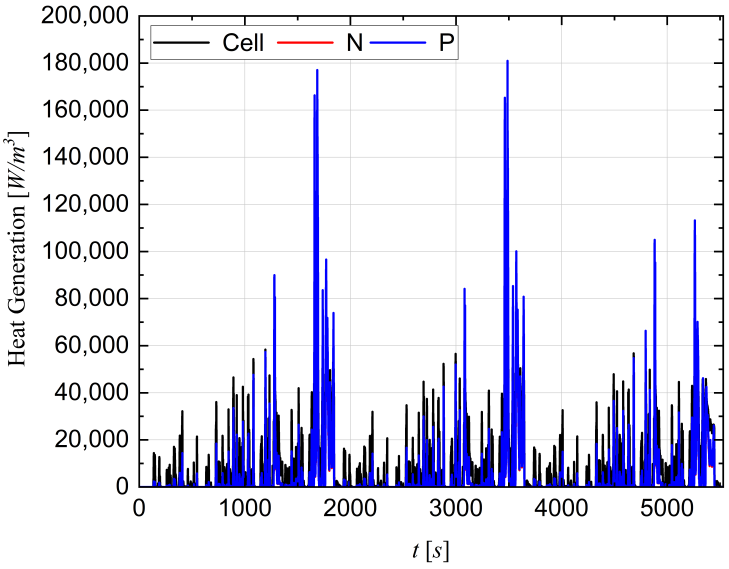

Figure 14. Heat generation of the LIB cells, negative and positive tabs under the WLTP class 3 drive cycle.

From Figure 15, it can be observed that when using CPCM-2, the LIB pack exhibits the highest temperature with the maximum temperature difference. The maximum temperatures with CPCM-1 and CPCM-3 show a relatively small difference, with the smallest temperature difference observed when using CPCM-1. In general, when employing these three CPCM types, the temperature difference of the battery pack does not exceed 5 degrees Celsius. Since the temperatures do not reach the melting point of the CPCM, the liquefaction rate for all three CPCM types is 0. The cooling performance of CPCM-1 and

CPCM-3 is similar, but considering the higher density of CPCM-1, choosing CPCM-3 is more reasonable from the perspective of light weighting electric vehicles.

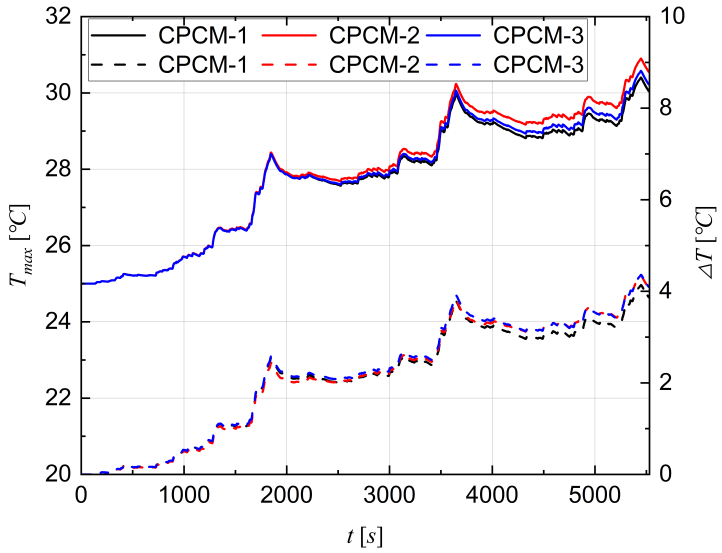

Figure 15. Results of configuration (4) BTMS under the WLTP class 3 drive cycle for three different CPCMs showing maximum temperature (solid lines) and temperature difference (dashed lines).

4.6. Cell Thermal Runaway Event

Building upon the foundation developed in the previous section, the BTMS system under the WLTP class 3 drive cycle is analysed in the event of one LIB cell failure in the pack using configuration (4) BTMS. For this investigation, the central battery in the LIB pack (cell 3) is set to have a thermal runaway occurring at about 1000 s, whilst the other fours cells work under the WLTP drive cycle. The temperature profile of cell 3—shown in Figure 16—is obtained from Yan et al. [40], and read to the Ansys Fluent 2023 R1 using UDF.

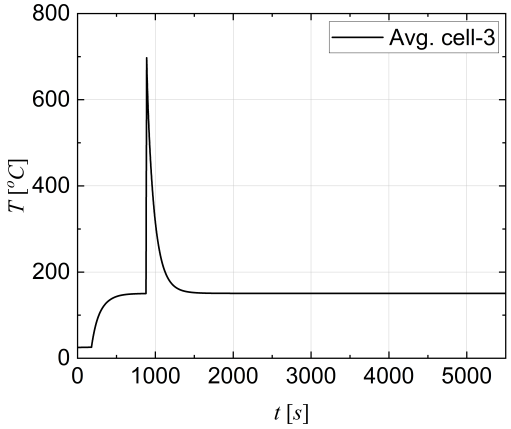

Figure 16. Temperature profile of cell 3 experiencing thermal runaway adapted with permission from [40].

The results for three CPCMs are depicted in Figure 17. The results from the simulation analysis indicate that, following the thermal runaway failure event in the middle LIB cell, the entire LIB pack experiences a rapid temperature increase. However, using configuration (4) suppresses thermal runaway occurrence in the other cells by keeping the average maximum cell temperature below 60 °C. It is worth nothing that due to relatively symmetric configuration of the LIB pack and the BTMS, the temperature profile of cell 1 and 5 as well as cell 2 and 4 are almost identical.

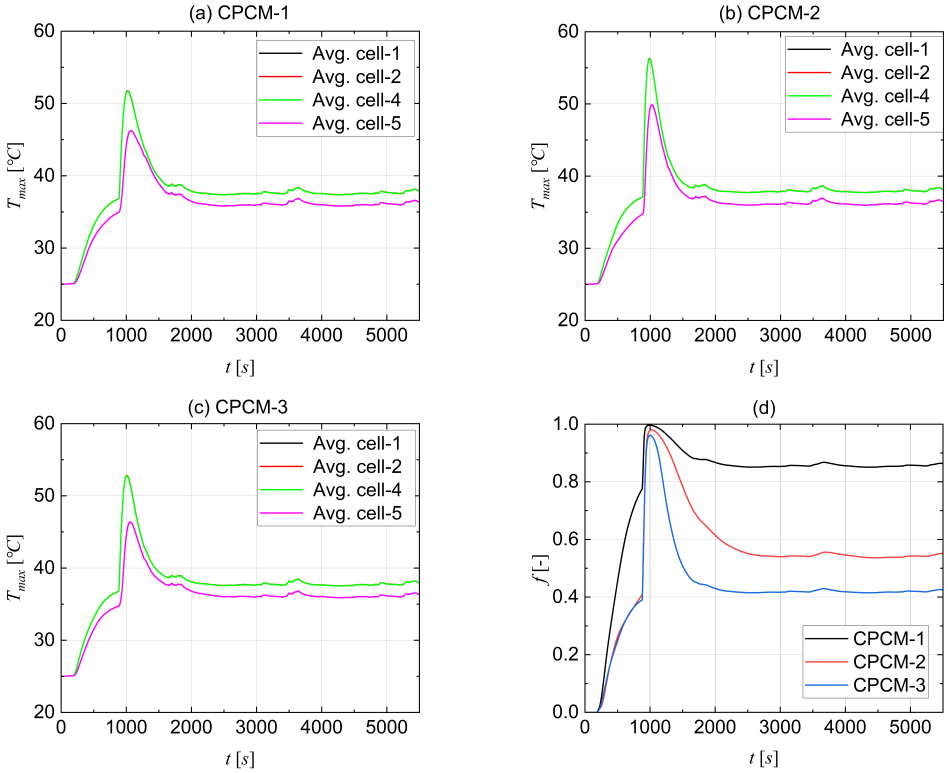

Figure 17. BTMS cooling performance in the event of thermal runaway under the WLTP class 3 drive cycle showing (**a**) CPCM-1, (**b**) CPCM-2, (**c**) CPCM-3, and (**d**) liquid fraction.

The use of CPCM-1—Figure 17a—results in the lowest maximum temperature and temperature difference, but it also exhibits the highest liquefaction rate. This is attributed to the CPCM-1's lower enthalpy change temperature at 32 °C. As shown in Figure 17b, when using CPCM-2, the LIB pack exhibits the highest maximum temperature. Despite the lower enthalpy change temperature of CPCM-2, its lower latent heat results in less heat absorption, leading to a decrease in the cooling performance of the BTMS. For CPCM-3, the higher enthalpy change temperature delays its activation, but due to its higher latent heat, the overall cooling performance of the BTMS is comparable to the use of CPCM-1—Figure 17c. Additionally, CPCM-3 exhibits a lower liquefaction rate, as depicted in Figure 17d. Therefore, through the this investigation, it is evident that the CPCM-3 is the best candidate during the thermal runaway event.

5. Conclusions

To tackle the safety challenges posed by LIB packs operating at high temperatures and high discharge rates, this study proposes a novel battery thermal management system (BTMS) that combines an S-shaped cooling channels with composite phase change materials (CPCM). Additionally, design configuration and energy consumption are optimised to enhance its overall efficiency. Furthermore, the study conducts simulations to evaluate the safety performance of the BTMS when active cooling becomes ineffective in a hybrid cooling setup. The optimised BTMS is further analysed under WLTP drive cycle as well as a thermal runaway event. The outcomes of this study can be briefly summarised as follows.

- Comparative simulation was conducted to assess the cooling effectiveness of three types of CPCMs for large-scale LIB pouch cells. Analysis shows that CPCM-3 is the best in terms of cooling performance, and thence, was selected as the passive cooling material for the rest of the study. The research findings indicate that the CPCM-3 enables the battery to operate safely.
- Four hybrid cooling configurations were established, and the results demonstrate that the configuration (4) can effectively limit the maximum internal temperature of the

battery pack to below 41.5 °C and the temperature difference to below 4.89 °C under an environmental temperature of 36 °C at a discharge rate of 3 C.

- Through numerical simulations of the coolant flow rate's impact on cooling performance and energy consumption, a flow rate of 0.1 m/s was selected as the optimal liquid flow rate for the current BTMS. Implementing this flow rate helps minimise the energy losses of the BTMS in EVs. Compared to various flow rate control strategies, adopting a single flow rate to control active cooling simplifies the operation. It reduces the likelihood of active cooling failure to a greater extent.
- Simulation results on BTMS cooling performance and liquid fraction when active cooling fails, specifically at a coolant flow rate of 0 m/s, indicate that the system with CPCM-3 can still operate safely.
- Using configuration (4), the battery pack can work safely under the WLTP class 3 drive cycle.
- In the case of thermal runaway for the middle cell, the proposed BTMS keeps the range of operational temperature below 60 °C, with CPCM-3 performing the best amongst three CPCMs.

Author Contributions: Conceptualisation, C.X., M.J. and E.H.; Software, C.X. and C.M.; Formal analysis, C.X.; Data curation, C.X. and M.J.; Writing–original draft, C.X.; Writing–review and editing, C.X., C.M., M.S., H.M., M.N.E., M.J. and E.H.; Supervision; M.J. and E.H. All authors have read and agreed to the published version of the manuscript.

Funding: This research received no external funding. For the purpose of open access, the author has applied a Creative Commons Attribution (CC BY) license to any Author Accepted Manuscript version arising from this submission.

Data Availability Statement: The original contributions presented in the study are included in the article, further inquiries can be directed to the corresponding author.

Conflicts of Interest: The authors declare no conflicts of interest.

References

1. Fotso-Nguemo, T.C.; Vondou, D.A.; Diallo, I.; Diedhiou, A.; Weber, T.; Tanessong, R.S.; Nghonda, J.P.; Yepdo, Z.D. Potential impact of 1.5, 2 and 3 C global warming levels on heat and discomfort indices changes over Central Africa. *Sci. Total Environ.* **2022**, *804*, 150099. [CrossRef] [PubMed]
2. Bibra, E.M.; Connelly, E.; Dhir, S.; Drtil, M.; Henriot, P.; Hwang, I.; Le Marois, J.B.; McBain, S.; Paoli, L.; Teter, J. Global EV Outlook 2022: Securing Supplies for an Electric Future. 2022. Available online: https://trid.trb.org/View/2005689 (accessed on 1 December 2023).
3. Wassiliadis, N.; Schneider, J.; Frank, A.; Wildfeuer, L.; Lin, X.; Jossen, A.; Lienkamp, M. Review of fast charging strategies for lithium-ion battery systems and their applicability for battery electric vehicles. *J. Energy Storage* **2021**, *44*, 103306. [CrossRef]
4. Tran, M.K.; Akinsanya, M.; Panchal, S.; Fraser, R.; Fowler, M. Design of a hybrid electric vehicle powertrain for performance optimization considering various powertrain components and configurations. *Vehicles* **2020**, *3*, 20–32. [CrossRef]
5. Piao, N.; Gao, X.; Yang, H.; Guo, Z.; Hu, G.; Cheng, H.M.; Li, F. Challenges and development of lithium-ion batteries for low temperature environments. *eTransportation* **2022**, *11*, 100145. [CrossRef]
6. Zhang, S.; Zhang, X. A multi time-scale framework for state-of-charge and capacity estimation of lithium-ion battery under optimal operating temperature range. *J. Energy Storage* **2021**, *35*, 102325. [CrossRef]
7. Osmani, K.; Alkhedher, M.; Ramadan, M.; Choi, D.S.; Li, L.K.; Doranehgard, M.H.; Olabi, A.G. Recent progress in the thermal management of lithium-ion batteries. *J. Clean. Prod.* **2023**, *389*, 136024. [CrossRef]
8. Park, S.H.; Park, J.; Ryou, M.H.; Lee, Y.M. Sensitivity of power of lithium-ion batteries to temperature: A case study using cylindrical-and pouch-type cells. *J. Power Sources* **2020**, *465*, 228238. [CrossRef]
9. Han, X.; Lu, L.; Zheng, Y.; Feng, X.; Li, Z.; Li, J.; Ouyang, M. A review on the key issues of the lithium ion battery degradation among the whole life cycle. *eTransportation* **2019**, *1*, 100005. [CrossRef]
10. Thakur, A.K.; Sathyamurthy, R.; Velraj, R.; Saidur, R.; Pandey, A.; Ma, Z.; Singh, P.; Hazra, S.K.; Sharshir, S.W.; Prabakaran, R.; et al. A state-of-the art review on advancing battery thermal management systems for fast-charging. *Appl. Therm. Eng.* **2023**, *226*, 120303. [CrossRef]
11. Xie, W.; Liu, X.; He, R.; Li, Y.; Gao, X.; Li, X.; Peng, Z.; Feng, S.; Feng, X.; Yang, S. Challenges and opportunities toward fast-charging of lithium-ion batteries. *J. Energy Storage* **2020**, *32*, 101837. [CrossRef]

12. Logan, E.; Dahn, J. Electrolyte design for fast-charging Li-ion batteries. *Trends Chem.* **2020**, *2*, 354–366. [CrossRef]
13. Liu, Y.; Zhu, Y.; Cui, Y. Challenges and opportunities towards fast-charging battery materials. *Nat. Energy* **2019**, *4*, 540–550. [CrossRef]
14. Zhang, Z.; Fu, L.; Sheng, L.; Ye, W.; Sun, Y. Method of liquid-cooled thermal control for a large-scale pouch lithium-ion battery. *Appl. Therm. Eng.* **2022**, *211*, 118417. [CrossRef]
15. Sait, H. Cooling a plate lithium-ion battery using a thermoelectric system and evaluating the geometrical impact on the performance of heatsink connected to the system. *J. Energy Storage* **2022**, *52*, 104692. [CrossRef]
16. Pan, S.; Ji, C.; Wang, S.; Wang, B. Study on the performance of parallel air-cooled structure and optimized design for lithium-ion battery module. *Fire Technol.* **2020**, *56*, 2623–2647. [CrossRef]
17. Lu, M.; Zhang, X.; Ji, J.; Xu, X.; Zhang, Y. Research progress on power battery cooling technology for electric vehicles. *J. Energy Storage* **2020**, *27*, 101155. [CrossRef]
18. Kleiner, J.; Singh, R.; Schmid, M.; Komsiyska, L.; Elger, G.; Endisch, C. Influence of heat pipe assisted terminal cooling on the thermal behavior of a large prismatic lithium-ion cell during fast charging in electric vehicles. *Appl. Therm. Eng.* **2021**, *188*, 116328. [CrossRef]
19. Huang, R.; Li, Z.; Hong, W.; Wu, Q.; Yu, X. Experimental and numerical study of PCM thermophysical parameters on lithium-ion battery thermal management. *Energy Rep.* **2020**, *6*, 8–19. [CrossRef]
20. Landini, S.; Leworthy, J.; O'Donovan, T. A review of phase change materials for the thermal management and isothermalisation of lithium-ion cells. *J. Energy Storage* **2019**, *25*, 100887. [CrossRef]
21. Wang, X.; Xie, Y.; Day, R.; Wu, H.; Hu, Z.; Zhu, J.; Wen, D. Performance analysis of a novel thermal management system with composite phase change material for a lithium-ion battery pack. *Energy* **2018**, *156*, 154–168. [CrossRef]
22. Zhi, M.; Fan, R.; Yang, X.; Zheng, L.; Yue, S.; Liu, Q.; He, Y. Recent research progress on phase change materials for thermal management of lithium-ion batteries. *J. Energy Storage* **2022**, *45*, 103694. [CrossRef]
23. Zhang, F.; Zhai, L.; Zhang, L.; Yi, M.; Du, B.; Li, S. A novel hybrid battery thermal management system with fins added on and between liquid cooling channels in composite phase change materials. *Appl. Therm. Eng.* **2022**, *207*, 118198. [CrossRef]
24. Zhao, Y.; Zou, B.; Ding, J.; Ding, Y. Experimental and numerical investigation of a hybrid battery thermal management system based on copper foam-paraffin composite phase change material and liquid cooling. *Appl. Therm. Eng.* **2023**, *218*, 119312. [CrossRef]
25. Zhang, W.; Liang, Z.; Yin, X.; Ling, G. Avoiding thermal runaway propagation of lithium-ion battery modules by using hybrid phase change material and liquid cooling. *Appl. Therm. Eng.* **2021**, *184*, 116380. [CrossRef]
26. Fan, Y.; Wang, Z.; Xiong, X.; Zhu, J.; Gao, Q.; Wang, H.; Wu, H. Novel concept design of low energy hybrid battery thermal management system using PCM and multistage Tesla valve liquid cooling. *Appl. Therm. Eng.* **2023**, *220*, 119680. [CrossRef]
27. Kong, D.; Peng, R.; Ping, P.; Du, J.; Chen, G.; Wen, J. A novel battery thermal management system coupling with PCM and optimized controllable liquid cooling for different ambient temperatures. *Energy Convers. Manag.* **2020**, *204*, 112280. [CrossRef]
28. Hosseinzadeh, E.; Genieser, R.; Worwood, D.; Barai, A.; Marco, J.; Jennings, P. A systematic approach for electrochemical-thermal modelling of a large format lithium-ion battery for electric vehicle application. *J. Power Sources* **2018**, *382*, 77–94. [CrossRef]
29. Chen, S.; Wan, C.; Wang, Y. Thermal analysis of lithium-ion batteries. *J. Power Sources* **2005**, *140*, 111–124. [CrossRef]
30. Jabbari, M.; Wang, R.; Liang, Z.; Esfahani, M.; Hosseinzadeh, E. Numerical modelling of nanocomposite conductive plate for battery thermal management using a novel multi-domain approach. *Appl. Therm. Eng.* **2021**, *182*, 116067. [CrossRef]
31. Dutil, Y.; Rousse, D.R.; Salah, N.B.; Lassue, S.; Zalewski, L. A review on phase-change materials: Mathematical modeling and simulations. *Renew. Sustain. Energy Rev.* **2011**, *15*, 112–130. [CrossRef]
32. Jaguemont, J.; Omar, N.; Van den Bossche, P.; Mierlo, J. Phase-change materials (PCM) for automotive applications: A review. *Appl. Therm. Eng.* **2018**, *132*, 308–320. [CrossRef]
33. Wang, R.; Liang, Z.; Souri, M.; Esfahani, M.; Jabbari, M. Numerical analysis of lithium-ion battery thermal management system using phase change material assisted by liquid cooling method. *Int. J. Heat Mass Transf.* **2022**, *183*, 122095. [CrossRef]
34. Malik, M.; Dincer, I.; Rosen, M.; Fowler, M. Experimental investigation of a new passive thermal management system for a Li-ion battery pack using phase change composite material. *Electrochim. Acta* **2017**, *257*, 345–355. [CrossRef]
35. Luo, X.; Guo, Q.; Li, X.; Tao, Z.; Lei, S.; Liu, J.; Kang, L.; Zheng, D.; Liu, Z. Experimental investigation on a novel phase change material composites coupled with graphite film used for thermal management of lithium-ion batteries. *Renew. Energy* **2020**, *145*, 2046–2055. [CrossRef]
36. Zhang, W.; Ling, G.; Zhuang, L.; Liang, Z. The effect of reducing the thermal contact resistance on the performance of battery thermal management system. *Int. J. Energy Res.* **2021**, *45*, 9970–9982. [CrossRef]
37. Zheng, Y.; Shi, Y.; Huang, Y. Optimisation with adiabatic interlayers for liquid-dominated cooling system on fast charging battery packs. *Appl. Therm. Eng.* **2019**, *147*, 636–646. [CrossRef]
38. Yu, L.; Zhang, J.; Wu, X.; Huang, J.; Hu, L.; Shi, L.; Dong, Y.; Chen, K.; Cao, B. Efficient optimization of parallel micro-channel heat sinks based on flow resistance network model. *Appl. Therm. Eng.* **2023**, *233*, 121169. [CrossRef]

39. Qian, Z.; Li, Y.; Rao, Z. Thermal performance of lithium-ion battery thermal management system by using mini-channel cooling. *Energy Convers. Manag.* **2016**, *126*, 622–631. [CrossRef]
40. Yan, H.; Marr, K.C.; Ezekoye, O.A. Thermal runaway behavior of nickel–manganese–cobalt 18650 lithium-ion cells induced by internal and external heating failures. *J. Energy Storage* **2022**, *45*, 103640. [CrossRef]